International Journal of Modelling and Simulation

ISSN: 0228-6203 (Print) 1925-7082 (Online) Journal homepage: www.tandfonline.com/journals/tjms20

Direct Torque Controlled Induction Motor Drive Based on Cascaded Three Two-Level Inverters

Thippiripati V. Kumar & Sandepudi S. Rao

To cite this article: Thippiripati V. Kumar & Sandepudi S. Rao (2014) Direct Torque Controlled Induction Motor Drive Based on Cascaded Three Two-Level Inverters, International Journal of Modelling and Simulation, 34:2, 70-82, DOI: 10.2316/Journal.205.2014.2.205-5849

To link to this article: https://doi.org/10.2316/Journal.205.2014.2.205-5849

DIRECT TORQUE CONTROLLED INDUCTION MOTOR DRIVE BASED ON CASCADED THREE TWO-LEVEL INVERTERS

Thippiripati V. Kumar* and Sandepudi S. Rao*

Abstract

In this paper, a new and an effective voltage switching-state algorithm to Direct Torque Control (DTC) of induction motor drive is proposed, which makes less torque and flux ripple at various operating frequency conditions. In conventional DTC, the torque and flux ripples are difficult to reduce as the applied voltage vector is independent of rotor speed especially at low speeds. To overcome this problem, the proposed technique introduces a voltage switching-state algorithm for four-level inversion using cascading three two-level inverters, in which choice of inverter voltage states is the function of rotor speed. From simulation results, the torque and flux ripple are decreased with proposed DTC when compared with the conventional DTC technique at various operating frequencies.

Key Words

Direct torque control, direct flux control, induction motor drive, four-level inverter

1. Introduction

In the recent past there has been a tremendous research in the Direct Torque Control (DTC) of Induction Motor (IM) drives. Conventional DTC envisages high dynamic performance and with an ease to control the torque and flux separately by choosing proper voltage switching states of inverter compared to Field-Oriented Control method. The choice of inverter voltage switching states restricts the torque and flux errors within the given hysteresis bands [1]–[3]. In conventional DTC, inverter operating switching frequency is uncontrolled and in turn depends on rotor speed, flux and torque hysteresis bands [4], [5]. To maintain the switching frequency as constant and independent of rotor speed, a new control technique using Space Vector Modulation (SVM)-DTC was proposed [6], which gives less torque and flux ripple. Further to reduce the flux and torque ripple various authors have proposed different techniques based on SVM [7]–[13]; but the design of proportional-integral (PI) controllers is complex. The alternative method is to solve the torque and flux ripple problem by using dithering technique [14]. But it requires high frequency triangle carrier signal. A control technique was proposed in [15] to reduce the torque and flux ripple without SVM technique. The switching frequency is uncontrolled which requires calculating several complicated equations in real time and also it requires high sampling frequency to reach the desired performance. In [16], the limitations of the stator flux and rotor speed estimation methods were discussed and a more accurate estimation method was proposed which has been concluded from sensitivity analysis. In [17], the authors use the fuzzy logic in estimating the motor parameters like stator and rotor resistance. However, flux and torque control are not considered in these papers. In [18], the authors proposed a soft starting method for IM with reduced energy losses using neuro fuzzy method. However, as this paper is confined to starting transients, the performance analysis in steady state has not been addressed. The DTC of sensorless IM has been discussed in [19]. The effective alternative method to reduce the flux and torque ripple is by using multilevel inverter topologies. The objective of the multilevel inverters is high power and voltage with less harmonics and optimum switching frequency. The three-level Neutral-Point-Clamped inverter-based DTC methods were suggested in [20], [21]. But their neutral point is fluctuating due to DC link capacitor current. This drawback was rectified by H-bridge topology, but it requires more than two isolated power supplies. Later, a new topology by cascading two two-level inverters was proposed in [22]. Using this cascaded topology an impressive DTC algorithm was proposed in

* Department of Electrical Engineering, National Institute of Technology, Waranagal, A.P. 506007, India; e-mail: tvinay.nitw@gmail.com, srinivasarao_nitw@yahoo.co.in

Recommended by Dr. M. Hamza
(DOI: 10.2316/Journal.205.2014.2.205-5849)

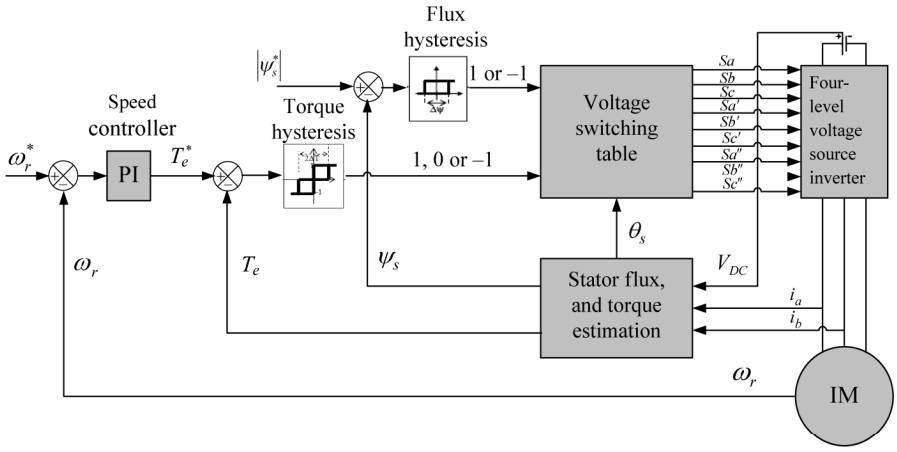

Figure 1. Proposed DTC scheme based on four-level inverter.

[23], but the selection of voltage vectors is inaccurate at low speed conditions.

In this paper, a four-level inverter is used to have a lesser dv/dt as compared to a two-level and three-level inverter, thereby decreasing the bearing current and shaft voltage problems. The objective of this research paper is to propose a better scheme for DTC IM drive to reduce torque ripple and flux ripple, develop mathematical models for the proposed scheme, carry out simulation studies on the proposed scheme and compare the simulation results of proposed scheme with existing scheme. The main contribution of this paper is that a new voltage switching table is designed for four-level inverter configuration by cascading three two-level inverters, method of selection of voltage switching states at various operating frequency conditions. Finally, it is noted that the torque and flux ripples impressively decrease when compared with the conventional DTC at various operating frequencies.

2. Proposed Four-Level Direct Torque Control (DTC) Method based on Cascaded Three Two-Level Inverters

The proposed four-level DTC-based IM drive is shown in Fig. 1, where ω_r^* is the speed reference in rad/s, ω_r is the actual rotor speed in rad/s, T_e^* is the reference torque generated from speed PI controller, T_e is the estimated torque in N-m, $|\psi_s^*|$ is the reference stator flux magnitude in Wb, ψ_s is the estimated stator flux magnitude in Wb, θ_s is the estimated stator flux angle, V_{DC} is the DC link voltage of the inverter, and i_a and i_b are the stator currents in amps.

The four-level inverter configuration is explained in the following section in detail.

2.1 Four-Level Inverter Configuration

The four-level inverter configuration by cascading three two-level inverters is shown in Fig. 2.

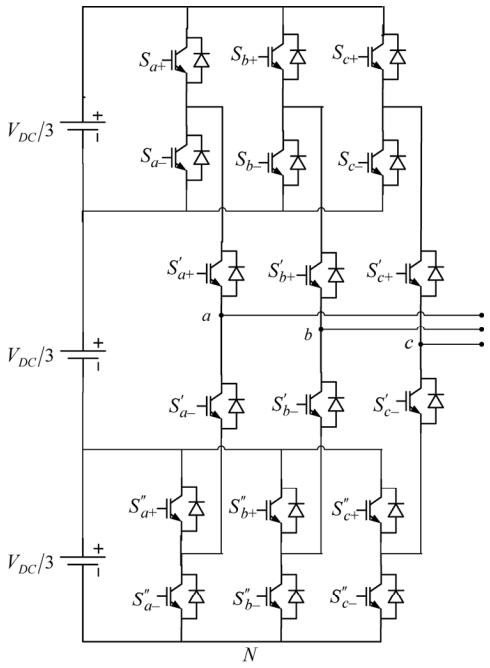

Figure 2. Four-level inverter configuration using cascading three two-level inverters.

The switching states for phase "a" are represented in Table 1.

Table 1
Switching State for Phase "a"

Switching States						Pole Voltage V_{aN}
S_{a+}	S_{a-}	S'_{a+}	S'_{a-}	S''_{a+}	S''_{a-}	
ON	OFF	ON	OFF	ON	OFF	V_{DC}
OFF	ON	ON	OFF	ON	OFF	$2V_{DC}/3$
ON	OFF	OFF	ON	ON	OFF	$V_{DC}/3$
ON	OFF	OFF	ON	OFF	ON	0

where S_{a+} is the first inverter "a" leg top switch, S'_{a+} is the second inverter "a" leg top switch and S''_{a+} is the third inverter "a" leg top switch.

Table 2 depicts the inverter individual states and the switches turned ON to realise those states, for the all three inverters.

Table 2
Switching State of Inverters 1, 2 and 3

Inverter 1			Inverter 2			Inverter 3			Voltage Space Vector
S_{a+}	S_{b+}	S_{c+}	S'_{a+}	S'_{b+}	S'_{c+}	S''_{a+}	S''_{b+}	S''_{c+}	
1	0	0	1	1	1	0	0	0	V_1
1	1	0	1	1	1	0	0	0	V_2
0	1	0	1	1	1	0	0	0	V_3
0	1	1	1	1	1	0	0	0	V_4
0	0	1	1	1	1	0	0	0	V_5
1	0	1	1	1	1	0	0	0	V_6
1	1	1	1	0	0	0	1	1	V_7
0	1	1	1	0	0	0	1	0	V_8
0	0	1	1	1	0	0	0	0	V_9
1	0	1	0	1	0	1	0	0	V_{10}
1	0	1	0	1	0	0	0	0	V_{11}
1	0	1	0	1	0	0	0	1	V_{12}
1	0	0	0	1	1	0	0	0	V_{13}
1	1	0	0	0	1	0	1	0	V_{14}
1	1	0	0	0	1	0	0	0	V_{15}
1	1	0	0	0	1	1	0	0	V_{16}
0	1	0	1	0	1	0	0	0	V_{17}
0	1	1	1	0	0	0	0	1	V_{18}
1	1	1	1	0	0	0	0	0	V_{19}
1	1	1	1	0	0	0	1	0	V_{20}
1	0	1	1	1	0	0	0	0	V_{21}
1	1	1	1	1	0	0	0	0	V_{22}
0	1	1	1	1	0	0	0	0	V_{23}
1	1	1	0	1	0	1	0	0	V_{24}
1	1	1	0	1	0	0	0	0	V_{25}
1	1	1	0	1	0	0	0	1	V_{26}
1	1	0	0	1	1	0	0	0	V_{27}
1	1	1	0	1	1	0	0	0	V_{28}
1	0	1	0	1	1	0	0	0	V_{29}
1	1	1	0	0	1	0	1	0	V_{30}
1	1	1	0	0	1	0	0	0	V_{31}
1	1	1	0	0	1	1	0	0	V_{32}
0	1	1	1	0	1	0	0	0	V_{33}
1	1	1	1	0	1	0	0	0	V_{34}
1	1	0	1	0	1	0	0	0	V_{35}
1	1	1	1	0	0	0	0	1	V_{36}
1	1	1	1	1	1	0	0	0	V_0

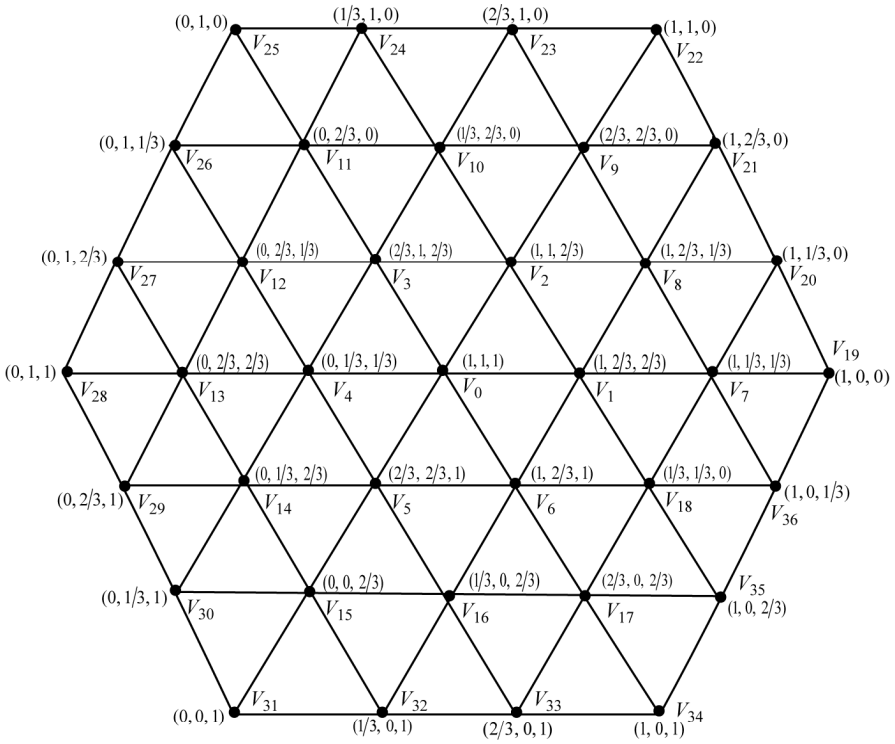

Figure 3. Voltage space vectors and their locations for a four-level inverter.

Figure 3 shows the states of the voltage space vectors for four-level configuration using cascading three two-level inverters. The four-level inverter produces 36 space vector locations.

An example is presented in this paragraph to determine the resultant space vector location for a combination (2/3, 2/3, 0) of the three inverters. The combination (2/3, 2/3, 0) implies that the switching state for inverter-1 is (0, 0, 1), for inverter-2 is (1, 1, 0) and for inverter-3 is (0, 0, 0), where "1" indicates that a upper switch in an inverter leg is turned ON and a "0" indicates that the lower switch is an inverter leg is turned ON. The resultant space vector V_s composed by the pole voltages V_{aN}, V_{bN} and V_{cN} is defined as:

$$V_s = V_{aN} + V_{bN} \cdot e^{j2\pi/3} + V_{cN} \cdot e^{j4\pi/3} \tag{1}$$

$$V_s = \frac{2}{3}V_{DC} + \frac{2}{3}V_{DC} \cdot e^{j2\pi/3} + 0 \tag{2}$$

From (2), it represents the (2/3, 2/3, 0) location, that is, V_9 vector, which is shown in Fig. 4.

Further, the resultant space vector (from Fig. 3) can be divided into 18 sectors for high frequency operation and 12 sectors for low and medium frequency operation. For high frequency operation, each sector occupies 20° (degrees) space location. Sector-1 indicates the space vector location from 350° to 10° with respect to α-axis, sector-2 indicates the space vector location from 10° to 30°, sector-3 indicates the space vector location from 30° to 50°, sector-4 indicates the space vector location from 50° to 70°, sector-5

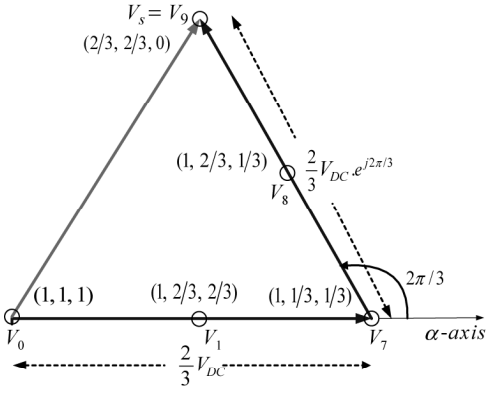

Figure 4. Realization of V_9 vector from all the three inverter states.

indicates the space vector location from 70° to 90°, sector-6 indicates the space vector location from 90° to 110°, sector-7 indicates the space vector location from 110° to 130°, sector-8 indicates the space vector location from 130° to 150°, sector-9 indicates the space vector location from 150° to 170°, sector-10 indicates the space vector location from 170° to 190°, sector-11 indicates the space vector location from 190° to 210°, sector-12 indicates the space vector location from 210° to 230°, sector-13 indicates the space vector location from 230° to 250°, sector-14 indicates the space vector location from 250° to 270°, sector-15 indicates the space vector location from 270° to 290°, sector-16 indicates the space vector location from 290° to 310°, sector-17 indicates the space vector location from 310° to 330° and sector-18 indicates the space vector location from

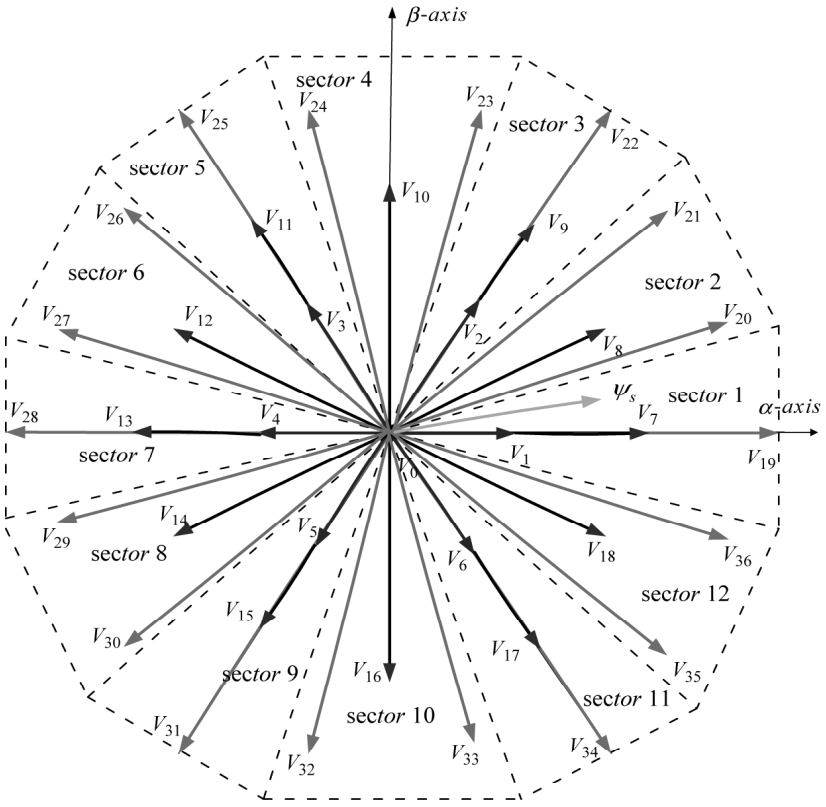

Figure 5. Voltage space vectors used for different frequency operations of four-level inverter DTC scheme.

330° to 350°. For low and medium frequency operation, each sector occupies 30° (degrees) space location, which is shown in Fig. 5. Sector-1 indicates the space vector location from 345° to 15° with respect to α-axis, sector-2 indicates the space vector location from 15° to 45°, sector-3 indicates the space vector location from 45° to 75°, sector-4 indicates the space vector location from 75° to 105°, sector-5 indicates the space vector location from 105° to 135°, sector-6 indicates the space vector location from 135° to 165°, sector-7 indicates the space vector location from 165° to 195°, sector-8 indicates the space vector location from 195° to 225°, sector-9 indicates the space vector location from 225° to 255°, sector-10 indicates the space vector location from 255° to 285°, sector-11 indicates the space vector location from 285° to 315° and sector-12 indicates the space vector location from 315° to 345°.

The analysis of the proposed method is explained under consideration of the stator flux space vector ψ_s is in sector-1 (space vector location from 350° to 10° for high frequency range and space vector location from 350° to 10° for low and medium frequency range). Based on the operating frequency of the inverter, the switching voltage vector states are divided into three parts namely high frequency, medium frequency and low frequency conditions.

2.1.1 High Frequency Operation (above 66% of the Rated Speed)

In high frequency range to control the torque and flux, the active voltage space vectors such as V_{19} to V_{36} and null vector V_0 are utilized to realize the resultant space vector. From Fig. 5, if the resultant stator flux vector ψ_s lies in sector-1, the stator flux magnitude can be increased by using V_{20}, V_{21}, V_{35} and V_{36} voltage vectors, whereas V_{24}, V_{25}, V_{32} and V_{31} voltage vectors are used to decrease the stator flux magnitude. Again in the same sector, the positive torque error can be reduced by choosing V_{21}, V_{22} and V_{23} voltage vectors, and negative torque error can be reduced by choosing V_{34}, V_{35} and V_{36} voltage vectors. In this frequency range, the choice of V_1–V_{18} voltage vectors is not preferable due to insufficient voltage magnitude to maintain the constant V/f ratio.

2.1.2 Medium Frequency Operation (between 33% and 66% of Rated Speed)

In medium frequency range to control the stator torque and flux, the active voltage space vectors such as V_7–V_{18} and null vector V_0 are utilized to realize the resultant space vector. From Fig. 5, if the resultant stator flux vector ψ_s lies in sector-1, the stator flux magnitude can be increased by using V_8, V_9, V_{17} and V_{18} voltage vectors, whereas V_{11}, V_{12}, V_{14} and V_{15} voltage vectors are used to decrease the stator flux magnitude. Again in the same sector, the positive torque error can be reduced by choosing V_8, V_9 and V_{10} voltage vectors, and negative torque error can be reduced by choosing of V_{16}, V_{17} and V_{18} voltage vectors. In this frequency range, the choice of V_1–V_6 voltage vectors is not preferable due to insufficient voltage magnitude to maintain the constant V/f ratio.

2.1.3 Low Frequency Operation (Less than 33% of the Rated Speed)

In low frequency range to control the stator torque and flux, the active voltage space vectors such as V_1–V_6 and null vector V_0 are utilized to realize the resultant space vector. From Fig. 5, if the resultant stator flux vector lies in sector-1, the stator flux magnitude can be increased by using V_2 and V_6 voltage vectors, whereas V_5 and V_3 voltage vectors are used to decrease the stator flux magnitude. Again in the same sector, the positive torque error can be reduced by choosing V_2 and V_3 voltage vectors, and negative torque error can be reduced by choosing V_5 and V_6 voltage vectors. In this frequency range, the choice of V_7 to V_{36} voltage vectors is not preferable due to insufficient voltage magnitude to maintain the constant V/f ratio.

2.2 Reduction of Flux Ripple and Torque Ripple Principle

The low flux and torque ripples are achieved based on the reduction of voltage ripple, because flux and torque ripples are functions of voltage. This voltage ripple technique is useful for low and medium operating frequencies. The inverter voltage equation can be expressed as:

$$v(k) = Ri_s + L_s di_s/dt + e_0 \tag{3}$$

where $v(k)$ is the output voltage of the inverter, and there are 36 locations of inverter output voltage vectors for four-level voltage source inverter, corresponding to the ON–OFF state of the inverter switching states shown in Table 2, e_0 is the induced voltage on the IM side, which depends on the operating frequencies (rotor speeds), L_s is the stator leakage inductance and i_s is the stator current.

Equation (3) can be written as:

$$di_s/dt = 1/L_s(v(k) - e_0) \tag{4}$$

where Ri_s drop is neglected.

Equation (4) shows that the rate of change in the stator current di_s/dt is determined by the selection of inverter voltage vector $v(k)$ for particular operating frequency. From (4), di_s/dt is the significant variable which controls the current harmonics in the steady state and the stator current response in the transient state. To get the low current ripple at steady state, it is required to select a suitable voltage vector such that Δi_s is minimum (from (4), $1/L_s(v(k) - e_0)$). From [24], the rotor flux can be written as:

$$\psi_r = (L_r/L_m)\psi_s - ((L_s L_r - L_m^2)/L_m)i_s \tag{5}$$

where ψ_s is the stator flux vector, ψ_r is the rotor flux vector, L_r is the rotor leakage inductance, L_s is the stator leakage inductance and L_m is the stator and rotor mutual inductance. Differentiating (5) with respect to time,

$$d\psi_r/dt = (L_r/L_m)d\psi_s/dt - \sigma di_s/dt \tag{6}$$

$$di_s/dt = [k_1 V_s - jk_2\psi_r\omega_r] \tag{7}$$

where $k_1 = L_r/\sigma L_m$ and $k_2 = 1/\sigma$.

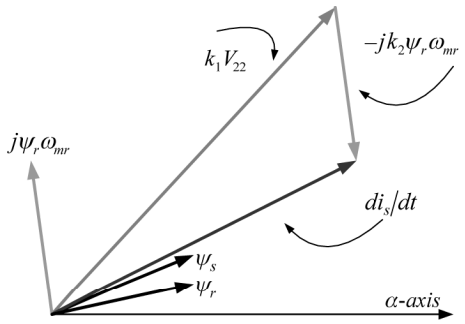

Figure 6. Incremental change in stator current to increase the flux and torque at high frequency operation.

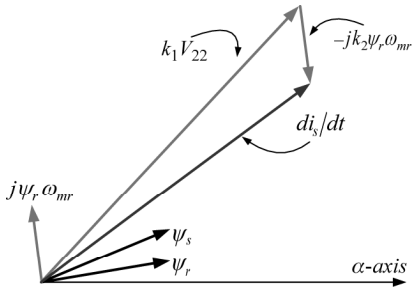

Figure 7. Incremental change in stator current to increase the flux and torque at medium frequency operation.

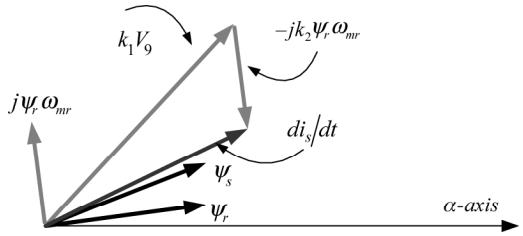

Figure 8. Incremental change in stator current to increase the flux and torque at medium frequency operation.

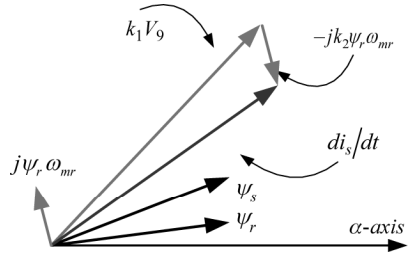

Figure 9. Incremental change in stator current to increase the flux and torque at low frequency operation.

From (7), di_s/dt is the rate of change in stator current, k_1V_s is the applied voltage vector and $jk_2\psi_r\omega_r$ is back e.m.f of the stator winding. The change in stator current di_s/dt depends on applied voltage and speed of rotor flux, and is independent of rotor flux magnitude. Rotor flux magnitude is maintained constant by choosing suitable inverter voltage vector. The back e.m.f $jk_2\psi_r\omega_r$ magnitude depends on rotor flux speed and independent of rotor flux magnitude. The rotor flux is maintained constant indirectly by controlling the stator flux using suitable voltage vector. Figures 6–10 give the deviation of the current ripple for different operating speeds. At high speed operating conditions, if the stator flux vector is assumed to

be in sector 1, then the required voltage vector magnitude should be high because it maintains V/f as constant. If voltage vector V_{23} is selected in the place of V_{22}, then load angle changes rapidly. Hence, V_{23} should not be applied to reduce the flux and torque errors for any position in sector-1. Depending on the rotor speed value, the selection of favourable voltage vectors to increase or decrease in the flux and torque ripple values are illustrated from Figs. 6 to 10.

For medium frequency operation, the choice of V_{22} voltage vector is not preferable to increase the flux and torque values in sector-1, because of current ripple di_s/dt increases which is shown in Fig. 7. To decreases the di_s/dt value, the V_9 voltage vector is more preferable than V_{22} voltage space vector, the variation of di_s/dt value after applying V_9 is shown in Fig. 8.

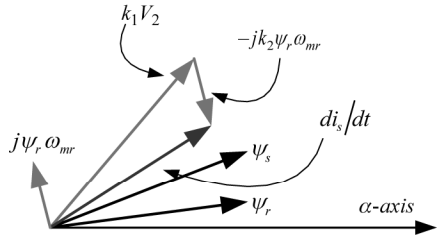

Figure 10. Incremental change in stator current to increase the flux and torque at low frequency operation.

For low operating frequency, the choice of V_9 voltage vector is not preferable to increase the flux and torque values in sector 1, because of current ripple di_s/dt increases which are shown in Fig. 9. To decreases the di_s/dt value under low speed conditions, the V_2 voltage vector is more preferable than the V_9 voltage space vector, the variation of di_s/dt value after applying V_2 is shown in Fig. 10. Depending on the rotor speed conditions, the selection of suitable voltage space vectors to increase or decrease the flux and the torque values are illustrated in Tables 3–5.

3. Simulation Results

After analysing, the mathematical and graphical picture of the proposed algorithm is applied to four-inverter configuration based on cascading three two-level inverters

Table 3
Choice of Active Vector for High Frequency Operation (above 66% of Rated Speed)

Flux Error	Torque Error	Sector Number																	
		1	2	3	4	5	6	7	8	9	10	11	12	13	14	15	16	17	18
>0	>0	V_{22}	V_{23}	V_{24}	V_{25}	V_{26}	V_{27}	V_{28}	V_{29}	V_{30}	V_{31}	V_{32}	V_{33}	V_{34}	V_{35}	V_{36}	V_{19}	V_{20}	V_{21}
	<0	V_{34}	V_{35}	V_{36}	V_{19}	V_{20}	V_{21}	V_{22}	V_{23}	V_{24}	V_{25}	V_{26}	V_{27}	V_{28}	V_{29}	V_{30}	V_{31}	V_{32}	V_{33}
<0	>0	V_{25}	V_{26}	V_{27}	V_{28}	V_{29}	V_{30}	V_{31}	V_{32}	V_{33}	V_{34}	V_{35}	V_{36}	V_{19}	V_{20}	V_{21}	V_{22}	V_{23}	V_{24}
	<0	V_{31}	V_{32}	V_{33}	V_{34}	V_{35}	V_{36}	V_{19}	V_{20}	V_{21}	V_{22}	V_{23}	V_{24}	V_{25}	V_{26}	V_{27}	V_{28}	V_{29}	V_{30}

Table 4
Choice of Active Vector for Medium Frequency Operation (between 33% and 66% of Rated Speed)

Flux Error	Torque Error	Sector Number											
		1	2	3	4	5	6	7	8	9	10	11	12
>0	>0	V_9	V_{10}	V_{11}	V_{12}	V_{13}	V_{14}	V_{15}	V_{16}	V_{17}	V_{18}	V_7	V_8
	<0	V_{17}	V_{18}	V_7	V_8	V_9	V_{10}	V_{11}	V_{12}	V_{13}	V_{14}	V_{15}	V_{16}
<0	>0	V_{11}	V_{12}	V_{13}	V_{14}	V_{15}	V_{16}	V_{17}	V_{18}	V_7	V_8	V_9	V_{10}
	<0	V_{15}	V_{16}	V_{17}	V_{18}	V_7	V_8	V_9	V_{10}	V_{11}	V_{12}	V_{13}	V_{14}

Table 5
Choice of Active Vector for Low Frequency Operation (Less than 33% of Rated Speed)

Flux Error	Torque Error	Sector Number											
		1	2	3	4	5	6	7	8	9	10	11	12
>0	>0	V_2	V_2	V_3	V_3	V_4	V_4	V_5	V_5	V_6	V_6	V_1	V_1
	<0	V_6	V_6	V_1	V_1	V_2	V_2	V_3	V_3	V_4	V_4	V_5	V_5
<0	>0	V_3	V_3	V_4	V_4	V_5	V_5	V_6	V_6	V_1	V_1	V_2	V_2
	<0	V_5	V_5	V_6	V_6	V_1	V_1	V_2	V_2	V_3	V_3	V_4	V_4

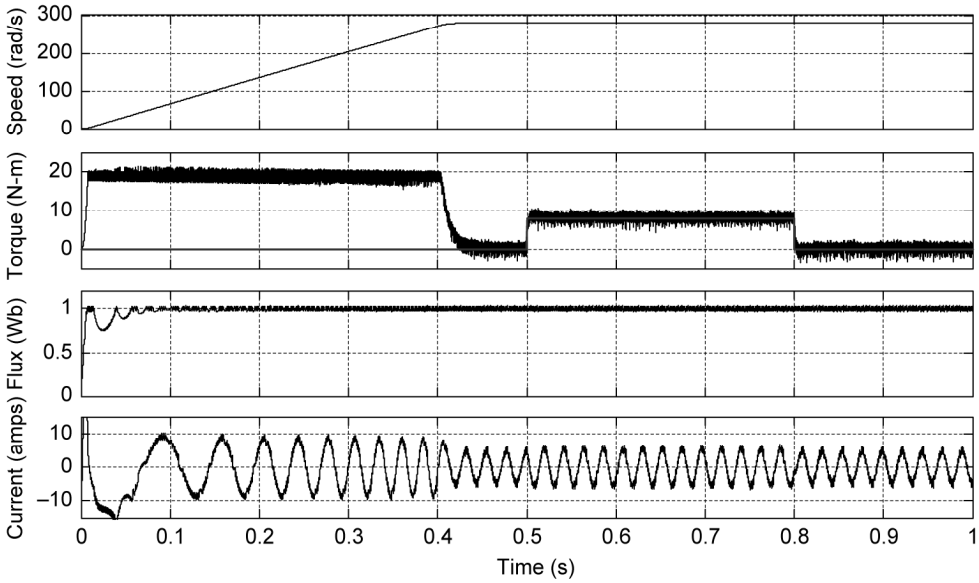

Figure 11. Simulation results of conventional DTC: (a) variation of rotor speed from 0 to 280 rad/s; (b) a load torque of 8 N-m is applied at 0.5 s and removed at 0.8 s; (c) stator flux; and (d) a-phase current I_a.

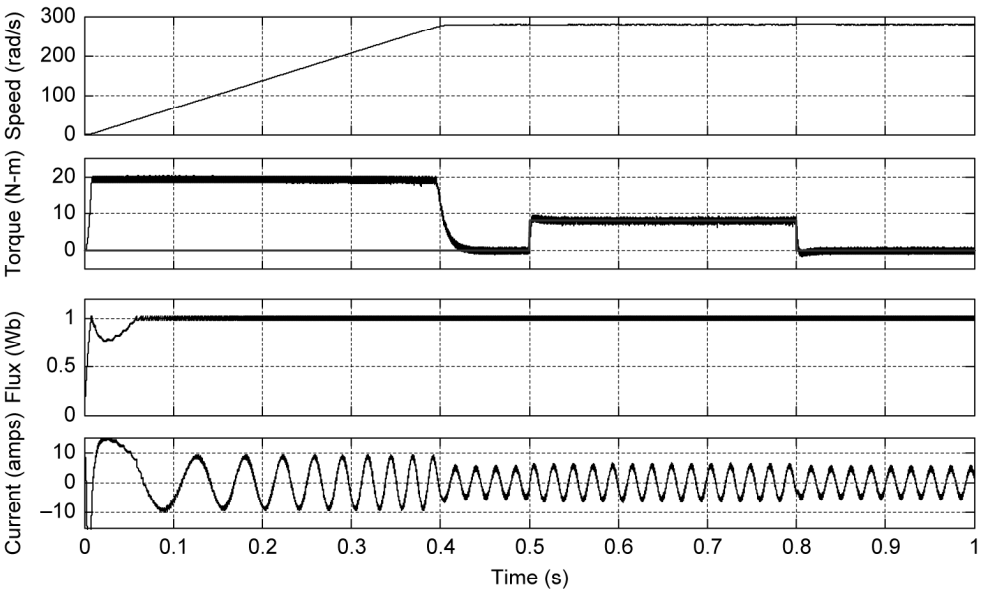

Figure 12. Simulation results of proposed DTC: (a) variation of rotor speed from 0 rpm to 280 rad/s; (b) a load torque of 8 N-m is applied at 0.5 s and removed at 0.8 s; (c) stator flux; and (d) a-phase current I_a.

simulated at different speed conditions for three-phase IM drive using MATLAB/SIMULINK. The steady-state and transient-state simulation results for conventional DTC and proposed DTC based on four-level inverter schemes are shown from Figs. 11 to 22. The simulations are carried out for various loads but the results are shown for 60% of rated load as a sample. Figures 11 and 12 show the forward motoring operation of IM drive at 280 rad/s for conventional DTC and proposed DTC schemes, respectively. Figures 13 and 14 show the torque and stator flux ripples at 280 rad/s rotor speed for conventional DTC and proposed DTC schemes, respectively. Figures 15 and 16 show the forward motoring operation of IM drive at 140 rad/s for conventional DTC and proposed DTC schemes, respectively. Figures 17 and 18 show the torque and stator flux ripples at 140 rad/s rotor speed for conventional DTC and proposed DTC schemes, respectively. Figures 19 and 20 show the forward motoring operation of IM drive at 40 rad/s for conventional DTC and proposed DTC schemes, respectively. Figures 21 and 22 show the torque and stator flux ripples at 40 rad/s rotor speed for conventional DTC and proposed DTC schemes, respectively.

The simulation results of motor operation are shown in Fig. 11, and Fig. 12 represents the motor speed at 280 rad/s, corresponding developed torque, stator flux and current for conventional DTC and proposed four-level DTC, respectively. From Fig. 14, an electromagnetic torque and flux ripple less compared with conventional DTC (Fig. 13) at 280 rad/s rotor speed is observed. Figures 15 and 16 represent the motor speed at 140 rad/s,

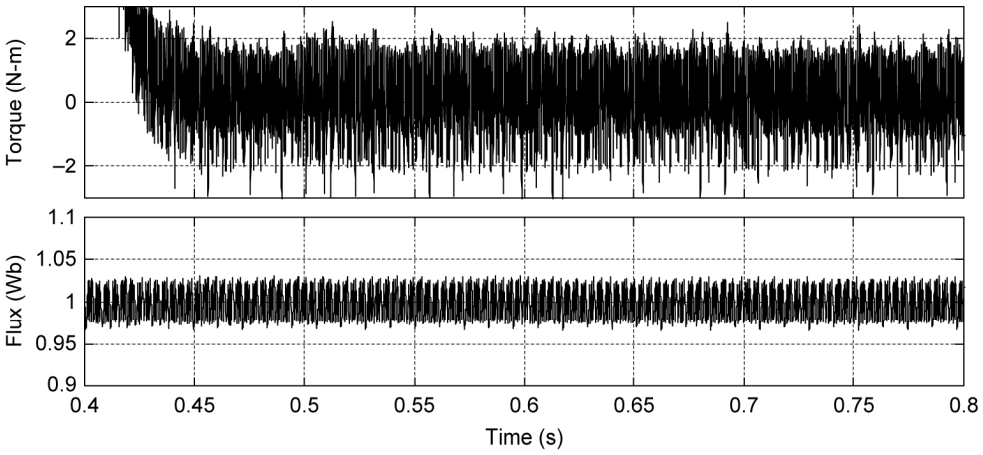

Figure 13. Simulation results of conventional DTC at 280 rad/s: (a) steady-state torque ripple in N-m and (b) steady-state flux ripple in Wb.

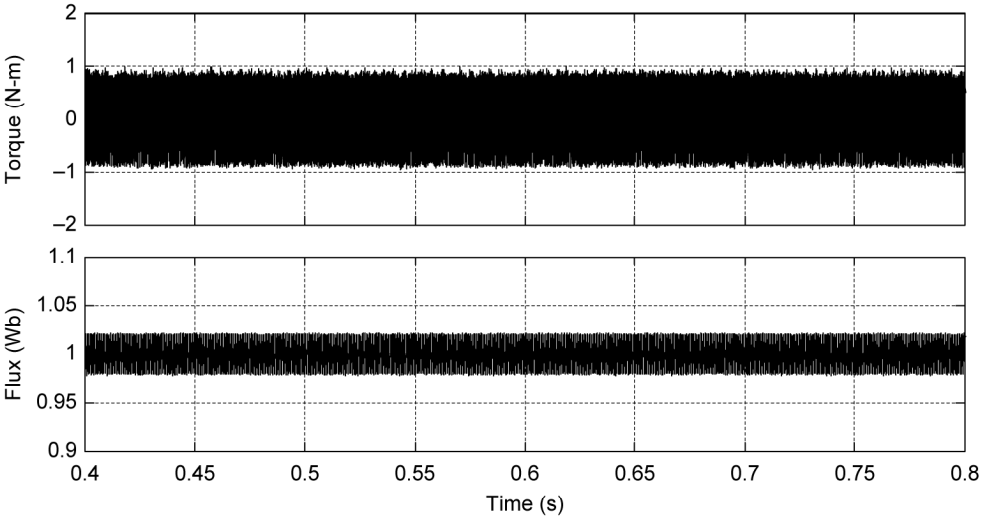

Figure 14. Simulation results of proposed DTC at 280 rad/s: (a) steady-state torque ripple in N-m and (b) steady-state flux ripple in Wb.

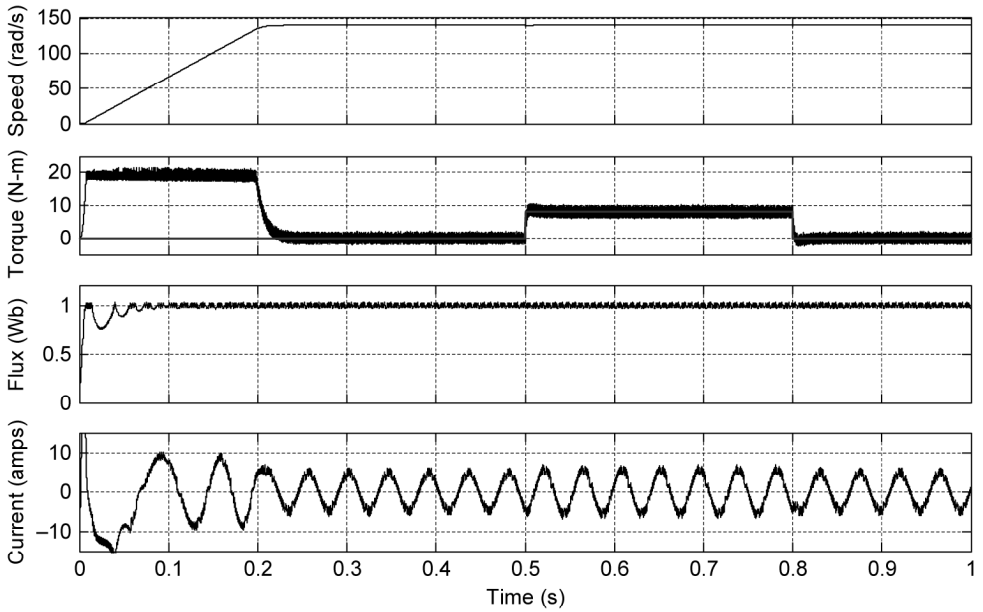

Figure 15. Simulation results of conventional DTC: (a) variation of rotor speed from 0 rpm to 140 rad/s; (b) a load torque of 8 N-m is applied at 0.5 s and removed at 0.8 s; (c) stator flux; and (d) a-phase current I_a.

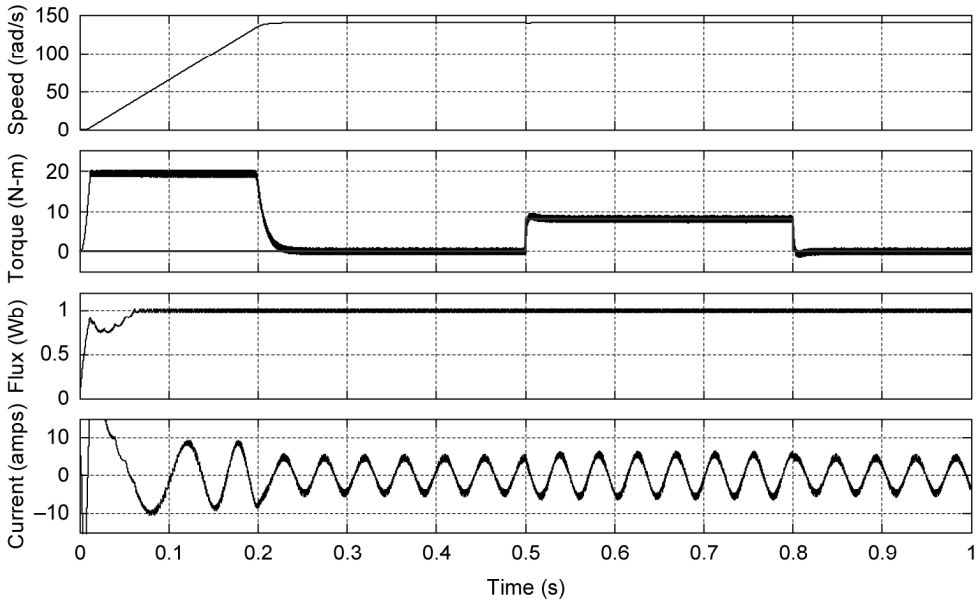

Figure 16. Simulation results of proposed DTC: (a) variation of rotor speed from 0 rpm to 140 rad/s; (b) a load torque of 8 N-m is applied at 0.5 s and removed at 0.8 s; (c) stator flux; and (d) a-phase current I_a.

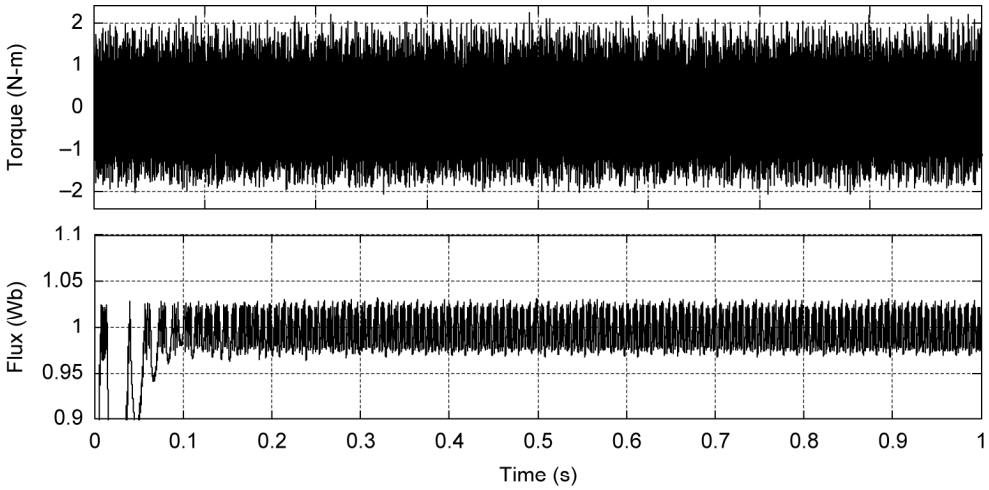

Figure 17. Simulation results of conventional DTC at 140 rad/s: (a) steady-state torque ripple in N-m and (b) steady-state flux ripple in Wb.

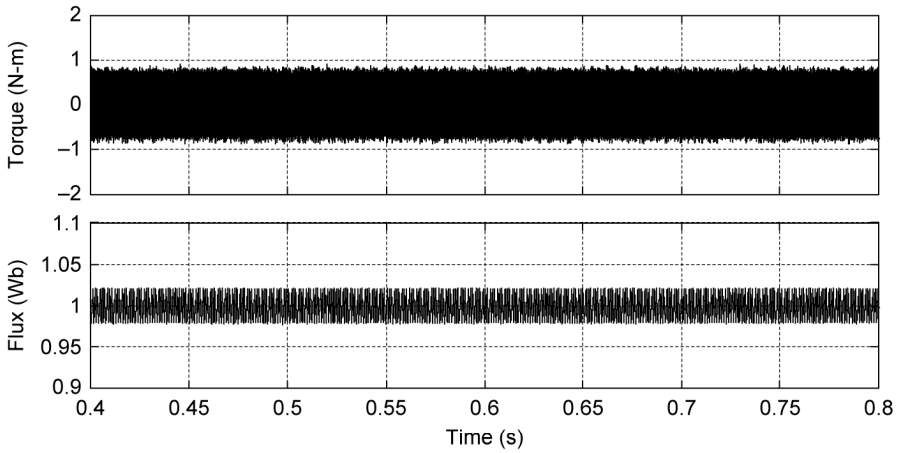

Figure 18. Simulation results of proposed DTC at 140 rad/s: (a) steady-state torque ripple in N-m and (b) steady-state flux ripple in Wb.

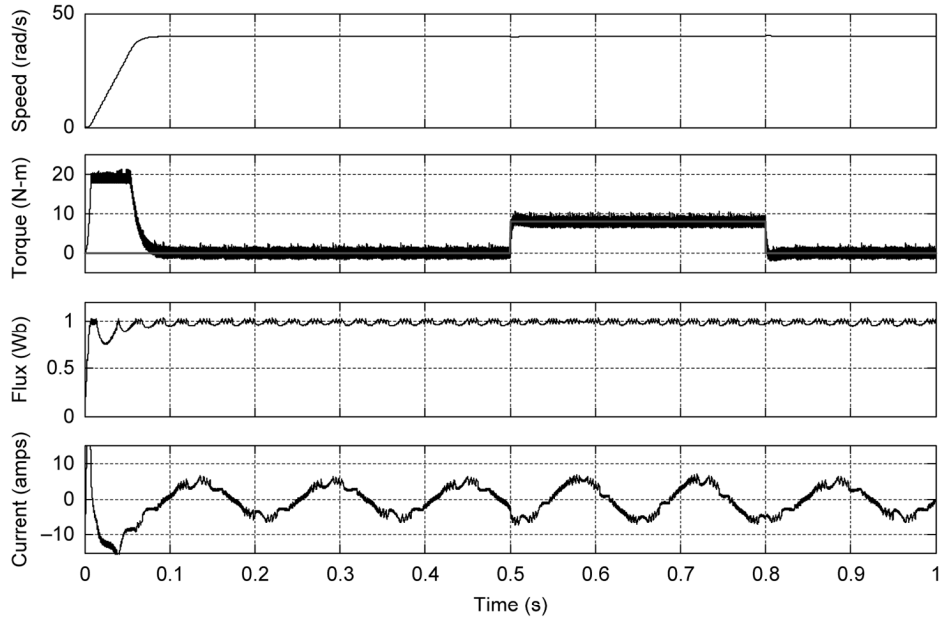

Figure 19. Simulation results of conventional DTC: (a) variation of rotor speed from 0 rpm to 40 rad/s; (b) a load torque of 8 N-m is applied at 0.5 s and removed at 0.8 s; (c) stator flux; and (d) a-phase current I_a.

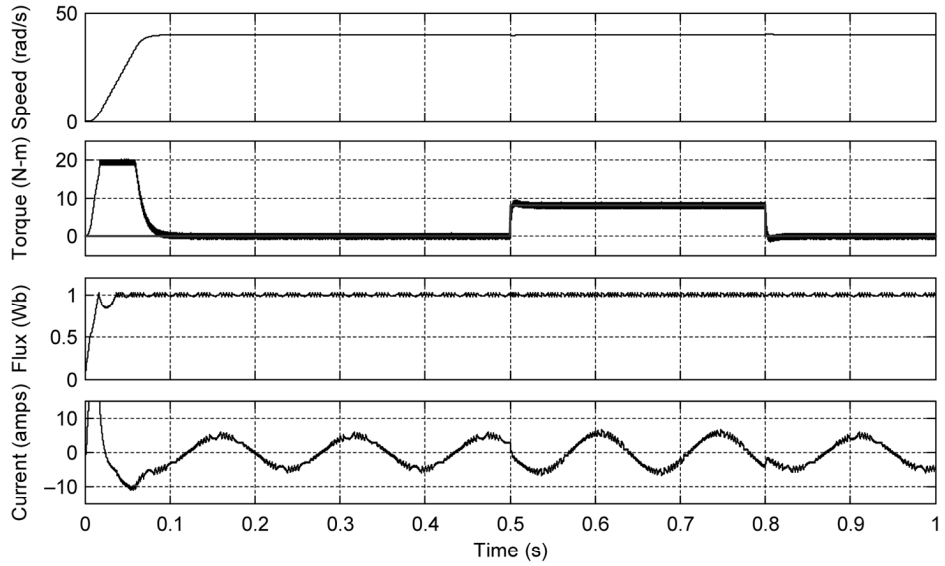

Figure 20. Simulation results of proposed DTC: (a) variation of rotor speed from 0 rpm to 40 rad/s; (b) a load torque of 8 N-m is applied at 0.5 s and removed at 0.8 s; (c) stator flux; and (d) a-phase current I_a.

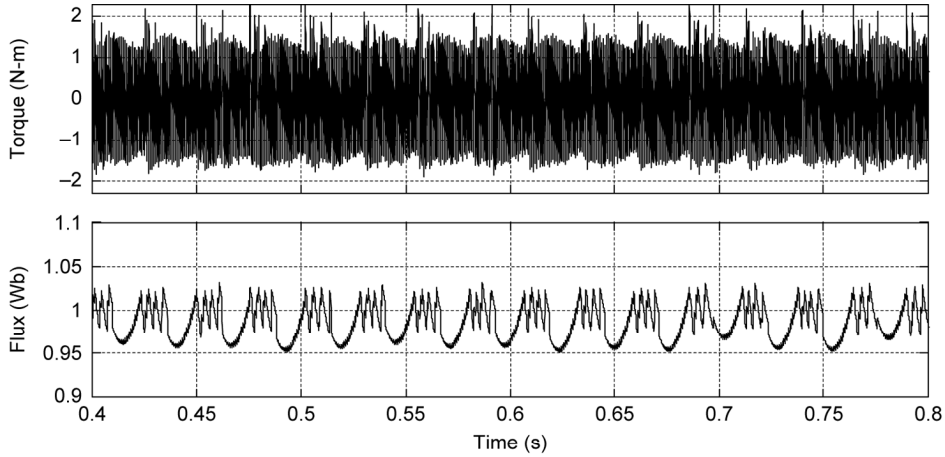

Figure 21. Simulation results of conventional DTC at 40 rad/s: (a) steady-state torque ripple in N-m and (b) steady-state flux ripple in Wb.

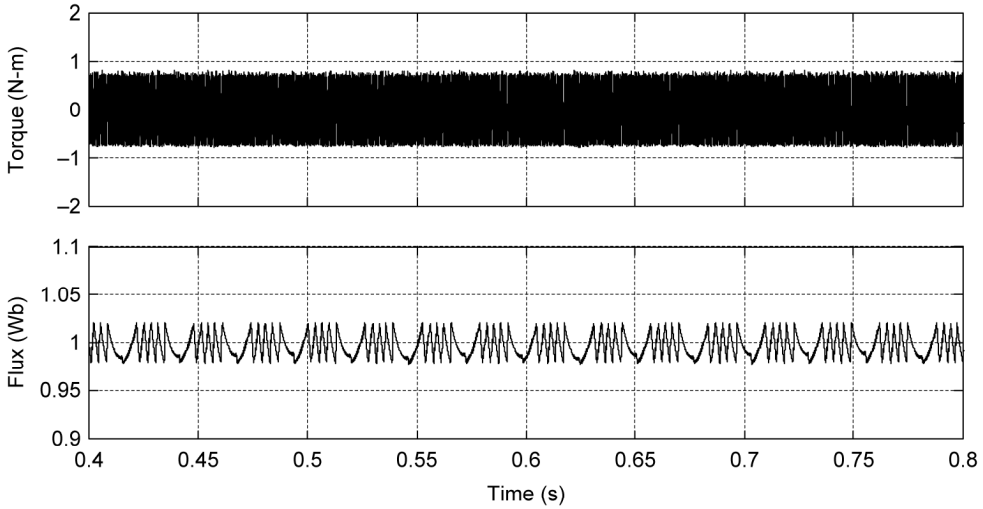

Figure 22. Simulation results of proposed DTC at 40 rad/s: (a) steady-state torque ripple in N-m and (b) steady-state flux ripple in Wb.

corresponding developed torque, stator flux and current for conventional DTC and proposed four-level DTC, respectively. From Fig. 18, an electromagnetic torque and flux ripple less compared with conventional DTC (*i.e.*, Fig. 17) at 280 rad/s rotor speed is observed. Figures 19 and 20 represent the motor speed at 40 rad/s, corresponding developed torque, stator flux and current for conventional DTC and proposed four-level DTC, respectively. From Fig. 22, it is observed that the electromagnetic torque and flux ripple are less when compared with the conventional DTC, that is, Fig. 21 at 40 rad/s rotor speed. From the above, at 280 rad/s (high speed), 140 rad/s (medium speed) and 40 rad/s (low speed) motor speeds the torque and flux ripples are minimized using proposed four-level-based DTC using cascading three two-level inverter, when compared with the conventional DTC method.

4. Conclusion

In this paper, a new voltage switching-state table is proposed to four-level inverter configuration by using cascading three two-level inverters for DTC of IM drive to reduce the flux and torque ripple at different operating frequencies. This control technique was tested at high, medium and low speed operating conditions. In all the operating frequency conditions, the flux ripple and torque ripple are decreased, when compared with the conventional DTC. Particularly at low speed operation, the proposed technique significantly reduced the flux ripple and torque ripple. Hence, the proposed technique ensures high performance in high power applications for low, medium and high speed operations.

References

[1] F. Blaschke, The principle of field-orientation as applied to the transvector closed-loop control system for rotating-field machines, *Siemens Review*, *34*, 1972, 217–220.

[2] I. Takahashi and T. Noguchi, A new quick-response and high-efficiency control of an induction motor, *IEEE Transactions on Industry Applications*, *22*(5), 1986, 820–827.

[3] D. Casadei, F. Profumo, G. Serra, and A. Tani, FOC and DTC: two viable schemes for induction motors torque control, *IEEE Transactions on Power Electronics*, *17*, 2002, 779–787.

[4] D. Telford, M.W. Dunnigan, and B.W. Williams, A comparison of vector control and direct torque control of an induction machine, *Proc. IEEE PESC'00*, Galway, 2000, 421–426.

[5] J.N. Nash, Direct torque control, induction motor vector control without an encoder, *IEEE Transactions on Industry Applications*, *33*, 1997, 333–341.

[6] J.-K. Kang and S.-K. Sul, New direct torque control of induction motor for minimum torque ripple and constant switching frequency, *IEEE Transactions on Industry Applications*, *35*(5), 1999, 1076–1082.

[7] T.G. Habetler, F. Profumo, M. Pastorelli, and L.M. Tolbert, Direct torque control of induction motor using space vector modulation, *IEEE Transactions on Industry Applications*, *28*, 1992, 1045–1053.

[8] X. Xu, R. DeDoncker, and D.W. Novotny, A stator flux oriented induction machine drive, *Proc. PESC I988 Conf. Rec.*, Kyoto, Japan, 1988, 870–876.

[9] X. Xue, X. Xu, T.G. Habetler, and D.M. Divan, A low cost stator flux oriented voltage source variable speed drive, *Proc. IEEE IAS Ann. Mtg. Conf. Rec.*, Seattle, WA, USA, 1990, 410–415.

[10] Y. Kumsuwana, S. Premrudeepreechacharna, and H.A. Toliyatb, Modified direct torque control method for induction motor drives based on amplitude and angle control of stator flux, *Electric Power Systems Research*, *78*(10), 2008, 1712–1718.

[11] T.V. Kumar and S.S. Rao, Modified direct torque control of three phase induction motor drives with low ripple in flux and torque, *Leonardo Journal of Sciences (LJS)*, *10*(18), 2011, 27–44.

[12] J. Zhang and M.F. Rahman, Analysis and design of a novel direct flux control scheme for induction machine, *Proc. Int. Conf. on IEMDC*, San Antonio, TX, 2005, 426–430.

[13] T.V. Kumar and S.S. Rao, Direct torque control method for induction motor drives based on modified amplitude and angle decoupled control of stator flux, *Proc. IEEE Conf. PEDES-2010*, India, December 2010.

[14] T. Noguchi, M. Yamamoto, S. Kondo, and I. Takahashi, Enlarging switching frequency in direct torque-controlled inverter by means of dithering, *IEEE Transactions on Industry Applications*, *35*(6), 1999, 1358–1366.

[15] S. Kuo-Kai, L. Juu-Kuh, P. Van-Truong, T. Thi-Thao, and S. Li-Jen, Evolution of local to global minimum torque ripples of direct torque control for induction motor drives, *T & F Journal of the Chinese Institute of Engineers*, *36*(5), 2012, 608–615.

[16] C. Korlinchaka and M. Comanescu, Robust sensorless sliding mode flux observer with speed estimate for induction motor

drives, *T & F Journal of Electric Power Components and Systems*, *40*(9), 2012, 1030–1049.
[17] D. Chatterjeea, A magnetization curve based stator resistance and fuzzy rotor resistance adaptation technique suitable for speed sensorless field-oriented control of induction machine, *T & F Journal of Electric Power Components and Systems*, *40*(16), 2012, 1789–1807.
[18] S.A.R. Kashif and M.A. Saqib, A neuro fuzzy application: soft starting of induction motors with reduced energy losses, *T & F Journal of Electric Power Components and Systems*, *40*(12), 2012, 1339–1350.
[19] M. Hajian, J. Soltani, and G.R. Arab Markadeh, Non-linear direct torque control of sensorless induction motor drives with parameter identification and capable for very low speeds, *T & F Journal of Electric Power Components and Systems*, *40*(15), 2012, 1656–1675.
[20] K.-B. Lee, J.-H. Song, I. Choy, and J.-Y. Yoo, Improvement of low-speed operation performance of DTC for three-level inverter-fed induction motors, *IEEE Transactions on Industry Electronics*, *48*(5), 2001, 1006–1014.
[21] S. Mukherjee and G. Poddar, Direct torque control of squirrel cage induction motor for optimum current ripple using three-level inverter, *IET Power Electronics*, *3*(6), 2010, 904–914.
[22] V.T. Somasekhar and K. Gopakumar, Three-level inverter configuration cascading two two-level inverters, *IEE Proceedings of Electric Power Applications*, *151*(2), 2003, 230–238.
[23] S.S. Rao and T.V. Kumar, Direct torque control of induction motor drives for optimum stator flux and torque ripple, *IEEE Proc. PEDS*, Singapore, 2011.
[24] A. Nabae, S. Ogasawara, and H. Akagia, Novel control scheme for current-controlled PWM inverters, *IEEE Transactions on Industry Applications*, *IA-22*(4), 1986, 696–701.

Biographies

Thippiripati V. Kumar received his B.Tech. degree in Electrical and Electronics Engineering from Jawaharlal Nehru Technological University, Hyderabad, India, in 2005 and M.Tech. degree from JNTU, Hyderabad, India, in 2008. Presently he is doing research in the power electronics and drives area at National Institute of Technology, Warangal, India.

Sandepudi S. Rao received his B.Tech. degree in Electrical Engineering from Regional Engineering College, Warangal, India, in 1992 and M.Tech. degree from Regional Engineering College, Calicut, India, in 1994. He obtained his Ph.D. degree from National Institute of Technology, Warangal, in 2007. Since 1996, he is working as a faculty member in National Institute of Technology, Warangal, India. He published many research papers in national, international journals and conferences. His research interests include power electronic drives, switch mode power converters, DSP controlled drives and renewable energy. He is a life member in System Society of India, Indian Society of Technical Education and member in Institution of Engineers (India).